International Journal of Heat and Technology
Vol. 44, No. 1, February, 2026, pp. 215-225
Journal homepage: http://iieta.org/journals/ijht

Evaluating Solar Cooling Performance Across Iraq Through Weather Data Simulation and System Modeling

Mohammed Taha Luhaibi*, Abdullah A. Badr, Ahmed Mustaffa Saleem, Ahmed Hani Ghanim

Technical Engineering College, Northern Technical University, Mosul 41002, Iraq

Corresponding Author Email: mohammed.taha@ntu.edu.iq

Copyright: ©2026 The authors. This article is published by IIETA and is licensed under the CC BY 4.0 license (http://creativecommons.org/licenses/by/4.0/).

https://doi.org/10.18280/ijht.440118

Received: 12 July 2025
Revised: 28 November 2025
Accepted: 9 December 2025
Available online: 28 February 2026

Keywords:
absorption cooling, $\bar{\phi}$–f chart method, solar air conditioning, solar energy, solar fraction, f-chart method

ABSTRACT

This study investigates the feasibility of implementing solar-driven absorption cooling systems in Iraq by employing the $\bar{\phi}$ −f chart method as a simplified computational tool for system design and simulation. The research analyzes key parameters influencing system performance, including collector area, glazing type, storage capacity, minimum load temperature, and collector tilt angle. Simulations were conducted for two major Iraqi cities (Baghdad and Mosul) using climate data from 2018 to 2022 to assess solar energy availability and system efficiency. Results demonstrate that double-glazed flat plate collectors significantly outperform single-glazed units, with optimal performance achieved at collector areas exceeding 55 m². The impact of thermal losses from storage tanks and heat exchangers was quantified, revealing substantial efficiency improvements as the collector area increases. Furthermore, the effect of optimizing the tilt angle and minimum load temperature is also evaluated and found to be minor in comparison to collector area and glazing type. It can be concluded that the simulation method shows that a properly designed solar thermal system could be applicable for the residential sector in Iraq to supply 100% solar fraction in the peak summer months.

1. INTRODUCTION

Interest in sustainable energy resources is growing worldwide due to the clean, environmentally benign, and readily available nature of the former, as well as its ability to contribute to sustainable development [1]. Designing efficient solar systems remains challenging due to the many factors affecting performance, such as collector characteristics, component parameters, and variable weather conditions. To ensure optimal operation, system design must balance component sizing with solar availability and load demand. Solar thermal design methods generally fall into two categories: Correlation-based and simulation-based approaches [2].

Various researchers have proposed and developed different methods based on correlation techniques for the development of solar water heating technologies. Klein [3] proposed a computational strategy for assessing the prolonged efficiency of thermal collectors, which functions under predetermined solar radiation thresholds identified for specific months. To address the limitations imposed by fixed critical parameters, Klein et al. [4] introduced the f-chart approach, enabling a rapid assessment of the long-term operational efficiency of solar energy configurations with typical designs. These systems are designed to supply thermal energy to the load while maintaining the load-side temperature of approximately 20 °C. Subsequently, Klein and Bechman [5] integrated the utilizability factor ($\bar{\phi}$) into the f-chart, resulting in the $\bar{\phi}$ −f chart-based design model for closed-loop solar thermal systems that function without operational constraints. Among all these models, $\bar{\phi}$ −f chart-based design model is considered one of the most widely adopted techniques currently used in the design for engineering solar thermal applications using correlation-based strategies. Additionally, improvements in computer power and the development of specific simulation tools like TRNSYS, WATSUN, POLYSUN, and SOLCHIPS have greatly increased the use of methods that focus on simulations [6-9].

Joudi and Abdul-Ghafour [10, 11] developed a TRNSYS-based dynamic model to evaluate solar-powered refrigeration performance in Iraqi residences and later introduced design charts to estimate the solar contribution in solar-assisted cooling systems. Alhadithie and Barwari [12] concentrated on evaluating the viability of utilizing solar-powered ventilation solutions in homes, considering the specific climatic conditions of the Iraqi Kurdistan region. In a related study, Dawood and Yousif [13] also used the f-chart framework to identify the most suitable configuration for a small capacity solar-powered absorption chiller for residential applications in Mosul. Furthermore, Abusaibaa et al. [14] investigated the feasibility of adopting a solar-assisted absorption cycle powered by Evacuated Tube Collectors (ETC) in Najaf, Iraq. The simulation-centered optimization helped in determining the most favorable system variables for the region and in proposing ways to enhance operational performance. The identified gap in this research area can be found in Iraq. Therefore, more research is required on the performance of solar cooling systems in Iraq. Prior Iraqi studies have mainly

examined single cities or used complex software tools such as TRNSYS. This study distinguishes itself by applying the simplified $\bar{\phi}-$f chart method, which is a straightforward computational approach to simulate and compare the performance of a solar energy system that driven absorption cooling system under two major Iraqi climates (Baghdad and Mosul) using multi-year meteorological data. A principal focus is on analyzing various parameters, including the collector glazing covers, collector area, specific storage capacity, minimum load temperature, and collector tilt angle. Furthermore, these parameters are compared across the different cities to evaluate their impact on system performance.

2. SYSTEM DESCRIPTION AND MODELLING

The $\bar{\phi}$–f chart method, as shown in Figure 1, is a well-established analytical approach utilized for evaluating closed-loop solar thermal systems. This methodology has its strength for the simulation of solar driven absorption refrigeration, industrial thermal processing, and space heating cases in which thermodynamic cycles are less affected by temperature variations of the heat source. It consists of a solar collector that captures solar radiation and transforms it into thermal energy. The collected heat is subsequently transferred to a thermal reservoir via a heat exchanger, which facilitates thermal energy transfer while ensuring that the working fluid in the solar circuit remains separated from the fluid stored in the reservoir. Afterward This heat is then supplied to a solar absorption system by a supply circuit with a supplementary heater, which is used to increase the system's temperature to a desired level once needed.

The $\bar{\phi}$–f chart is a computational method used to model solar heating and cooling systems. It was developed as a hybrid between the f-chart and utilizability methods. It has been used as a design method for sizing flat-plate collector fields and estimating monthly system efficiency. This method has shown to be particularly useful for absorption cooling systems to achieve stable thermal input to the generator and to maintain the minimum temperature for efficient chiller operation. The proportion of the monthly energy demand met by solar thermal systems incorporating auxiliary heating elements in parallel configurations [5] is determined using typical daily performance data for each respective month through a standardized analytical expression.

$$f_{tl} = \bar{\phi}_{max}\, Y - 0.015[exp(3.85\, f_{tl})][1 - exp(-0.15\, X)]\, R_s^{0.76} \quad (1)$$

The relation defines the ratio between the nominal storage heat capacity per collector area, and the actual storage capacity is expressed as:

$$R_s = \frac{350}{M \times cp / A_c} \quad (2)$$

X and Y, as nondimensional variables, are expressed by the following relations:

$$Y = \frac{A_c\, F_R(\tau\alpha)_n \frac{(\overline{\tau\alpha})}{(\tau\alpha)_n} \bar{H}_t\, N}{Q_L} \quad (3)$$

$$X = \frac{A_c\, F_R\, U_L \Delta t\, (100\,^{\circ}C)}{Q_L} \quad (4)$$

The mean daily utilizability [3] can be determined by the formula below:

$$\bar{\phi} = \frac{f_{tl}}{Y} \quad (5)$$

where, the average utilizability is linked to the maximum utilizability and the clearance index $\bar{K}_t$ through the function $\bar{\phi} = \bar{\phi}\,(X_{C,min})$.

$$\begin{gathered} \bar{\phi}_{max} = exp[\bar{X}_c + C\,\bar{X}_c^2]\left[A + B\left(\frac{R_n}{\bar{R}}\right)\right] \\ A = a_0 + a_1\bar{K}_t + a_2\bar{K}_t^2 \\ B = b_0 + b_1\bar{K}_t + b_2\bar{K}_t^2 \\ C = c_0 + c_1\bar{K}_t + c_2\bar{K}_t^2 \end{gathered} \quad (6)$$

The coefficients in the above equation are obtained from Table 1.

The nondimensional critical radiation ratio is defined as follows:

$$\bar{X}_c = \frac{I_c}{r_{t,n}\, R_n\, \bar{K}_T\, \bar{H}_o} \quad (7)$$

The ratio of critical radiation is given by the following equation:

$$I_C = \frac{F_R U_L(\bar{T}_i - \bar{T}_{avg})}{F_R(\tau\alpha)_n \frac{(\overline{\tau\alpha})}{(\tau\alpha)_n}} \quad (8)$$

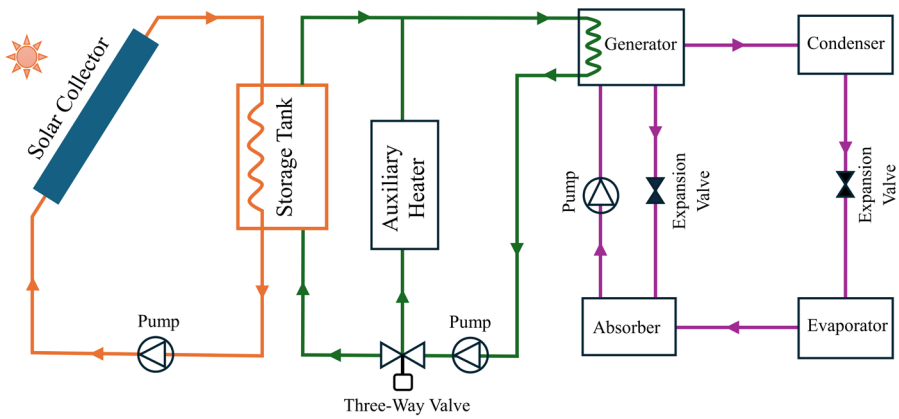

Figure 1. Proposed solar cooling system

The minimum non-dimensional critical radiation ratio $\bar{X}_{C,min}$ is derived using the equation above under the condition that the inlet temperature equals the minimum required temperature, thereby determining the lowest average monthly value of critical radiation. The solar energy fraction, as calculated through the aforementioned relations, must be adjusted to reflect the impact of thermal inefficiencies arising from the storage tank, as well as the thermal resistance introduced by the heat exchanger, which separates the storage unit from the thermal load. These inefficiencies lead to a rise in the actual operating temperature at the collector inlet, and as a result, contribute to a reduction in the system's effective solar contribution.

The tank's average temperature [5] is calculated using:

$$\bar{T}_s = \frac{\bar{T}_i + \bar{T}_{min}}{2} \tag{9}$$

The reduction in usable energy temperature caused by the presence of a heat exchanger can be quantified by the following equation:

$$\bar{T}_i = \frac{f Q_L}{\varepsilon_L C_{min} \Delta t} + \bar{T}_{min} \tag{10}$$

The rate at which the storage tank loses energy to the environment, evaluated at $\bar{T}_{env}$.

$$Q_{st} = (UA)_{st}(\bar{T}_s - \bar{T}_{env}) \tag{11}$$

If the environmental temperature and storage $(UA)_{st}$ value are steady for a month, integrating over that month gives:

$$Q_{st} = (UA)_{st}(\bar{T}_s - \bar{T}_{env})\,\Delta t \tag{12}$$

where, Q_{st} and $\bar{T}_s$ are the monthly average tank losses and storage temperature, respectively. Therefore, the system's total load consists of the absorption cooling load plus storage tank heat loss.

$$Q_t = Q_{st} + Q_L \tag{13}$$

The fraction represents the portion of the total load fulfilled by solar energy is obtained as:

$$f = f_{tl}\left(1 + \frac{Q_{st}}{Q_L}\right) - \frac{Q_{st}}{Q_L} \tag{14}$$

The total solar heat delivered over a month is:

$$Q_{solar} = f.Q_t \tag{15}$$

The auxiliary heater's energy contribution is calculated as follows:

$$Q_{ah} = (1 - f)\,Q_t \tag{16}$$

To simulate the solar system, it is essential to calculate the following fundamental values, starting with the monthly total load, which is given by:

$$Q_L = Q_g.3600.hrs.N \tag{17}$$

The average daily global solar radiation [15] for the month, as received on the collector surface, is given by:

$$\bar{H}_t = \bar{R}\,.\,\bar{H} \tag{18}$$

The monthly average daily irradiance on a tilted surface, normalized to the horizontal, is given by the following relation:

$$\bar{R} = \left(1 - \frac{\bar{H}_d}{\bar{H}}\right)\bar{R}_b + \frac{\bar{H}_d}{\bar{H}}\left(\frac{1+\cos\beta}{2}\right) + \rho\left(\frac{1-\cos\beta}{2}\right) \tag{19}$$

The ratio of monthly-mean daily beam flux on an inclined surface versus a horizontal surface is expressed as:

$$\bar{R}_b = \frac{\cos(\lambda-\beta)\cos\delta\sin\omega_{ss} + \frac{\pi}{180}\omega_{ss}\sin(\lambda-\beta)\sin\delta}{\cos\lambda\cos\delta\sin\omega_s + \frac{\pi}{180}\omega_s\sin\lambda\sin\delta} \tag{20}$$

where, δ is the declination angle, which is given by:

$$\delta = 23.45\sin\left[\frac{360}{365}(n + 284)\right] \tag{21}$$

For a horizontal plane, the sunset hour angle is determined by:

$$\omega_s = \cos^{-1}[-\tan\delta\ \tan\lambda] \tag{22}$$

While ω_{ss} represents the sunset hour angle for a surface oriented toward the equator, calculated as:

$$\omega_{ss} = min\begin{cases}\omega_s \\ \cos^{-1}[-\tan\lambda\tan(\lambda-\beta)]\end{cases} \tag{23}$$

The formulation for computing the monthly average daily clearness index is as follows:

$$\bar{K}_t = \frac{\bar{H}}{\bar{H}_o} \tag{24}$$

The term $\bar{H}_o$ corresponds to the monthly-averaged daily extraterrestrial irradiance received by a horizontal surface and is determined using:

$$\bar{H}_o = \frac{86400}{\pi} I_{gc}\left[\cos\lambda\cos\delta\sin\omega_s + \frac{\pi}{180}\omega_s\sin\lambda\sin\delta\right] \tag{25}$$

where, I_{gc} represent the extraterrestrial irradiance over a specified day:

$$I_{gc} = I_{sc}\left[0.033\cos\left(\frac{360\,n}{365}\right) + 1\right] \tag{26}$$

Building on daily diffuse correlations, Erbs et al. [16] established empirical models for the monthly average diffuse fraction, which can be obtained by:

$$\frac{\bar{H}_d}{\bar{H}} = d_0 + d_1\bar{K}_t + d_2\bar{K}_t^2 + d_3\bar{K}_t^3 \quad for\ \omega_s \le 81.4°\ and\ 0.3 \le \bar{K}_t \le 0.8 \tag{27a}$$

$$\frac{\bar{H}_d}{\bar{H}} = e_0 + e_1\bar{K}_t + e_2\bar{K}_t^2 + e_3\bar{K}_t^3 \quad for\ \omega_s > 81.4°\ and\ 0.3 \le \bar{K}_T \le 0.8 \tag{27b}$$

The coefficients in Eq. (26) are obtained from Table 1.

The incidence angle modifier throughout the day can be estimated by considering the solar incidence angle at 14:30 h solar time on a south-facing (equator-facing) collector. Thus, the monthly average incidence angle modifier for the solar collector is calculated as presented by Reddy [17].

$$\frac{(\overline{\tau\alpha})}{(\tau\alpha)_n} = \left(\bar{R}_b \frac{\bar{H}_b}{\bar{H}_t}\right)\left[\left[1+\psi\left(\frac{1}{cos\theta_b}-1\right)\right]+\left[\frac{\bar{H}_d(1+cos\theta_b)+\bar{H}\,\rho\,(1-cos\theta_b)}{2\bar{H}_t}\right](1+\psi)\right] \quad (28)$$

The parameter ψ denotes the coefficient used in the incidence angle modifier formulation, is set to -0.11 for collectors with single glazing and -0.17 for those with double glazing.

The solar beam incidence angle θ_b on the collector plane [15] is given by:

$$cos\theta_b = \cos(\phi-\beta)\cos\lambda\cos\omega + \sin\lambda\ \sin(\phi-\beta) \quad (29)$$

This ratio $r_{t,n}$ quantifies the noon-time monthly average hourly global radiation as a portion of the monthly mean daily global radiation on a horizontal plane:

$$r_{t,n} = r_{d,n}[1.07 + 0.025\sin(\omega_s - 60)] \quad (30)$$

where, $r_{d,n}$ denotes the ratio of the monthly average hourly diffuse irradiance to the corresponding monthly mean daily diffuse radiation on a horizontal surface.

$$r_{d,n} = \frac{\pi}{24}\left[\frac{1-\cos\omega_s}{\sin\omega_s - \frac{\pi}{180}\omega_s\cos\omega_s}\right] \quad (31)$$

The ratio of beam radiation on an inclined surface to that on a horizontal surface of south facing surface at solar noon for the northern hemisphere is:

$$R_{b,n} = \frac{\cos|\lambda-\delta-\beta|}{\cos|\lambda-\delta|} \quad (32)$$

The noon-time ratio of solar radiation received on a tilted surface to that on a horizontal surface for a typical day of the month is expressed as:

$$R_n = \left(1-\frac{r_{d,n}}{r_{t,n}}\frac{\bar{H}_d}{\bar{H}}\right)R_{b,n} + \left(\frac{1+\cos\beta}{2}\right)\left(\frac{r_{d,n}}{r_{t,n}}\right)\left(\frac{\bar{H}_d}{\bar{H}}\right) + \rho\left(\frac{1-\cos\beta}{2}\right) \quad (33)$$

Table 1. Coefficients of Eqs. (6) and (27)

j	a_j	b_j	c_j	d_j	e_j
0	2.943	-4.345	-0.170	1.391	1.311
1	-9.271	8.853	-3.061	-3.560	-3.022
2	4.031	-3.602	2.936	4.189	3.427
3				-2.137	-1.821

3. RESULTS AND DISCUSSION

3.1 INTRODUCTION

A computational simulation of the solar system was performed using a program developed within the Engineering Equation Solver (EES) environment [18] employing the $\bar{\phi}$–f chart methodology to study the performance of solar thermal system delivers hot water to power an absorption cooling system operates for 10 hours per day and 7 days per week that requiring a generator thermal load of 12000 W at a minimum load temperature of 75–85 °C during May to September. one and two-glass cover flat plate solar collectors (FPCs) are used coupled with a well-insulated storage tank and an auxiliary heater set in parallel, an appropriate value has been assigned for a performance parameter of properly designed solar collector. The collector is set at an (λ-15)° inclination angle facing south, where λ is the latitude and is equal to 33.5° and 36.19° for Baghdad and Mosul, respectively. The relevant input parameters used for the simulation are presented in Table 2, while Figure 2 illustrates the computational flow of the model, showing input data, system processes, and outputs.

Klein and Beckman [5] validated the $\bar{\phi}$–f chart against TRNSYS simulations, as shown in Figure 3. The comparison reveals that the solar fraction values obtained from the $\bar{\phi}$–f Chart method closely match those produced by TRNSYS, indicating that the $\bar{\phi}$–f chart method offers a reliable estimate of solar fraction for the specified months.

The climatic data from the Iraqi Agricultural Meteorological Center [19] have been used in this work based on the average data between 2018–2022, for Baghdad, and Mosul cities.

The mean monthly incoming solar radiation on a horizontal surface is shown in Figure 4, while Figures 5 and 6 illustrate the temperature distribution in Iraq from May to September for the same period.

Table 2. The input parameters for running the performance tests of the solar cooling system

Description	Values of Parameters
Selective surface flat plate (FPC) with single glass cover [20]	$F_R(\tau\alpha)_n$ = 0.75 $F_R\,U_L$ = 5 (W/m^2·°C)
Selective surface flat plate (FPC) with double glass cover [21]	$F_R(\tau\alpha)_n$ = 0.8 $F_R\,U_L$ = 3.6 (W/m^2·°C)
Storage tank's total thermal conductance	$(UA)_s$ = 11.1 W/°C [13]
Specific storage capacity	STC = 83.5 kg/m^2 [5]
Generator load	Q_g = 12000 W
Useful energy temperature at the minimum value	T_{min} = 80 °C

3.2 Effect of collector type

The solar fraction variation for single- and double-glazed flat plate collectors across Baghdad and Mosul is demonstrated in Figures 7 and 8. These figures aim to determine how different types of glazing affect flat plate collector performance across varying collector areas from May to September in Iraq. The results depict that the mean solar fraction increases with larger collector areas, and double-glazing consistently outperforms single-glazing for all cities. However, the percentage improvement of using double glazing decreases as the collector area increases. According to simulation results, double glazing reaches its maximum relative improvement over single glazing at a collector area of 40 m², which results in advancements of 39.4% in Baghdad and 40.8% in Mosul. The smallest improvement rates appear at 55 m² with performance gains of 32.9% for Baghdad, while Mosul registers 34.1%. The performance enhancements with double glazing reach their highest levels during May across all studied months, with peak improvements at 46.5% in Baghdad, followed by 47.2% in Mosul. July shows the poorest performance at 55 m², with performance enhancements of 27.8% in Baghdad, and Mosul sees a 30.7% improvement. The implementation of double-glazing collectors results in increased solar fraction averages of 36.2% in Baghdad and 37.5% in Mosul throughout all conditions, thus demonstrating

their strong performance in Iraq's climate conditions, which allows them to reach a solar fraction of 100% during June through August for areas exceeding 55 m².

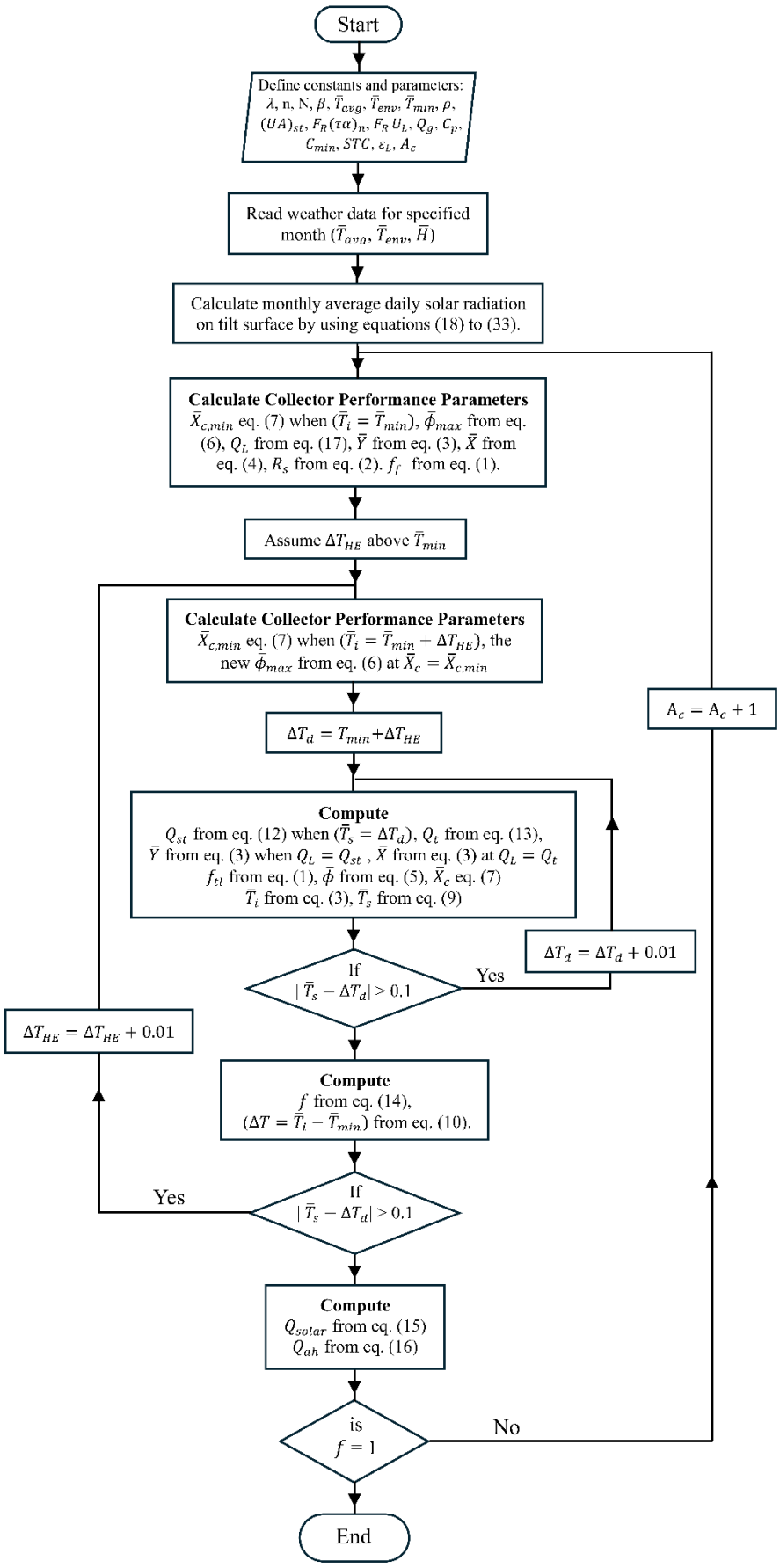

Figure 2. The flow chart for the calculation procedure

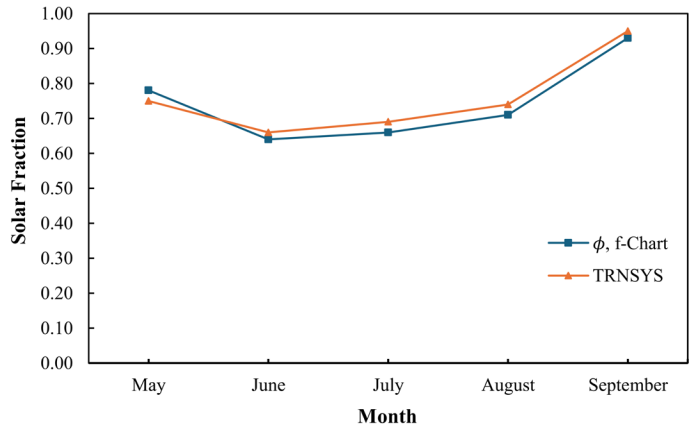

Figure 3. Solar fraction validation with TRNSYS

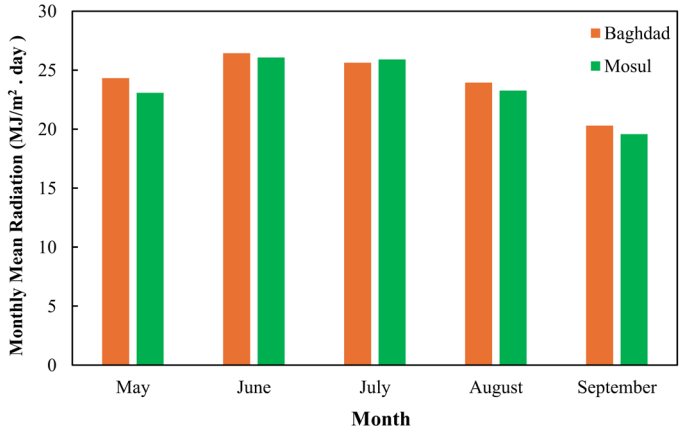

Figure 4. Monthly average solar intensity on a horizontal surface from 2018 to 2022

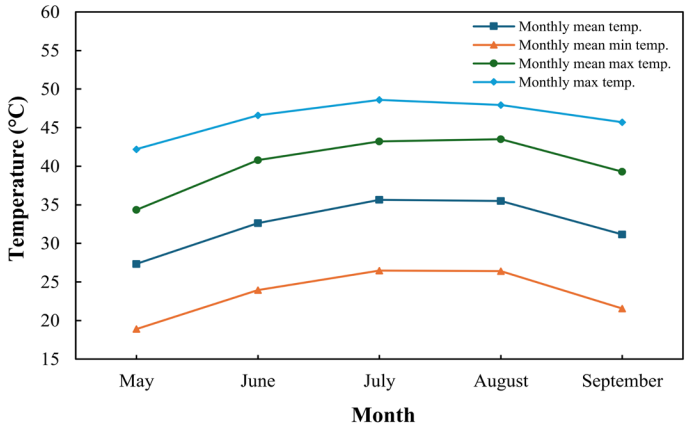

Figure 5. Monthly average temperature variation with months in Baghdad from 2018 to 2022

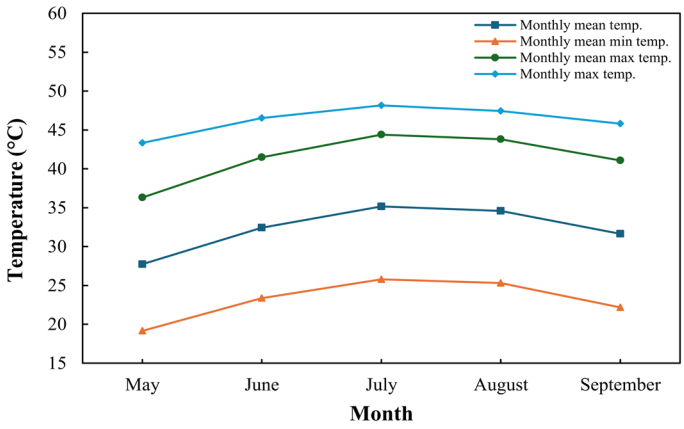

Figure 6. Monthly average temperature variation with months in Mosul from 2018 to 2022

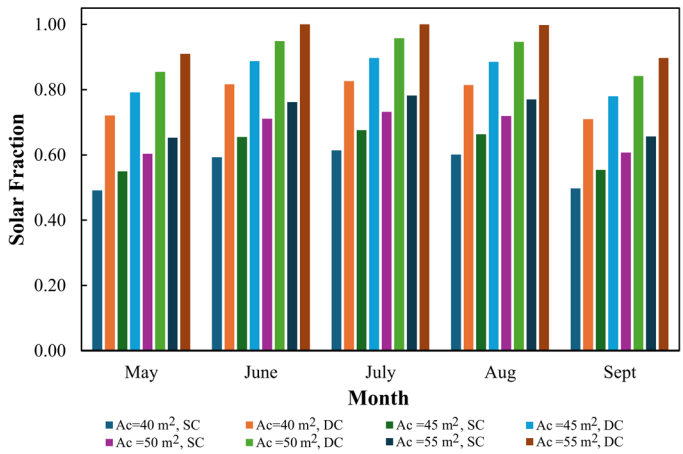

Figure 7. Solar fraction variation with months for single- and double-glazing covers for Baghdad

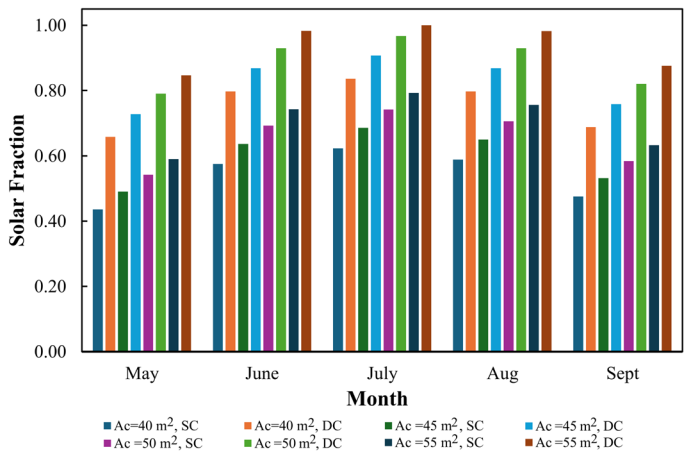

Figure 8. Solar fraction variation with months for single- and double-glazing covers for Mosul

3.3 Effect of system losses

The depicted Figures 9 and 10 show how solar fraction varies when analyzing different loss factors, which include combined storage tank and heat exchanger losses (f) and solar fraction (f_{tl}), which only comprises storage tank losses, along with solar fraction (f_f) that excludes losses for double-glazed flat plate collectors in Baghdad and Mosul, respectively. These figures aim to analyze how these losses were affected by different collector area sizes during the months of May through September, given Iraq's weather conditions. The findings show that greater collector areas lead to substantial reductions in losses from storage tanks and heat exchangers. Baghdad's percentage of storage tank loss diminishes from about 8.98% when the area is 40 m² to 3.24% at 55 m², and the total losses drop from 11.24% to 3.60% for the same area increase. Mosul experiences a decrease in average tank loss percentage from 9.26% at 40 m² to 4.09% at 55 m², and combined losses reduce from 11.91% to 4.71%. The average tank and heat exchanger losses experience reductions of

approximately 68% in Baghdad and 60% in Mosul when the collector area is increased. The observed reductions lead to maximum solar fraction performance increases of 23.62% in Baghdad, while Mosul sees 24.13%. The collector area of 55 m² demonstrates the most significant benefits as combined losses reach their minimum and solar fraction performance peaks. The results indicate that the storage tank losses are the dominant part of combined losses; in addition, increasing collector areas produces significant performance improvements by reducing storage and heat exchanger losses, which leads to higher solar fraction efficiency.

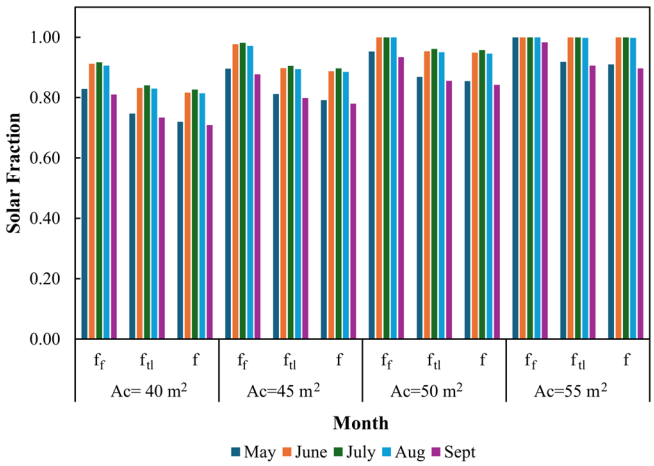

Figure 9. Solar fraction variation with losses at different collector areas for Baghdad

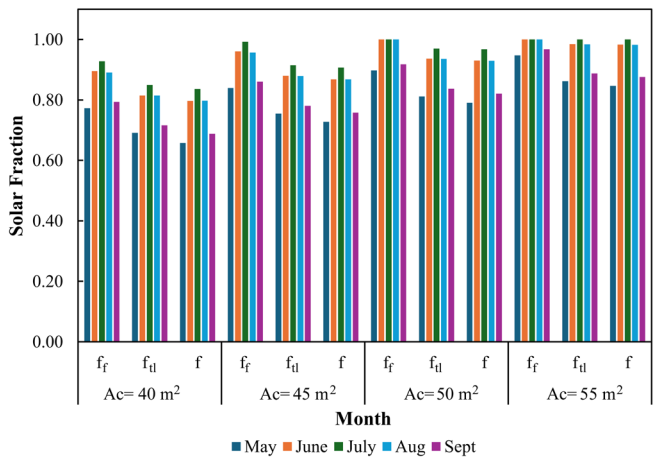

Figure 10. Solar fraction variation with losses at different collector areas for Mosul

3.4 Effect of minimum load temperature

Figures 11 through 14 present the variation in solar fraction and storage tank temperature of the double-glazing collector from May to September, considering different required minimum load temperatures to operate the generator for the absorption cooling system in Baghdad and Mosul. It was observed that increasing the minimum load temperature generally resulted in a rise in the storage tank temperature, with an average increase of 4.2% for Baghdad and 4.5% for Mosul for each 5 °C increment. However, this rise in storage temperature was accompanied by a corresponding decrease in solar fraction, which dropped by an average of 9.3% for Baghdad and 11.3% for Mosul under the same conditions.

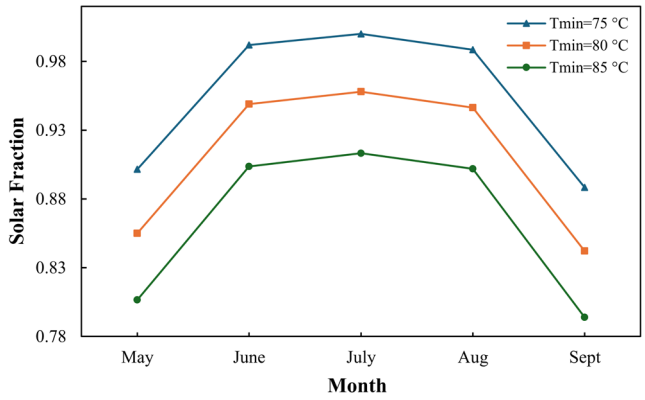

Figure 11. Solar fraction variation with months at different minimum load temperatures for Baghdad

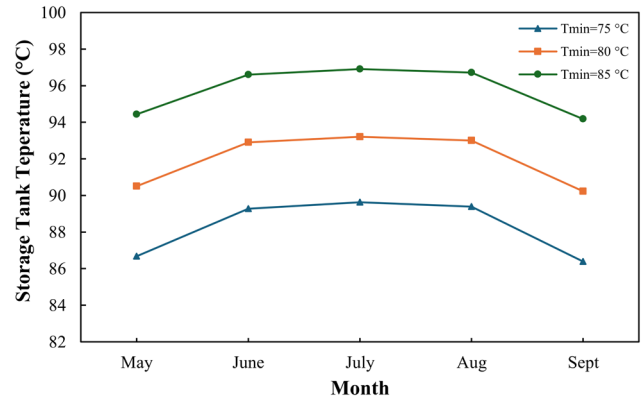

Figure 12. Storage tank temperature variation with months at different minimum load temperatures for Baghdad

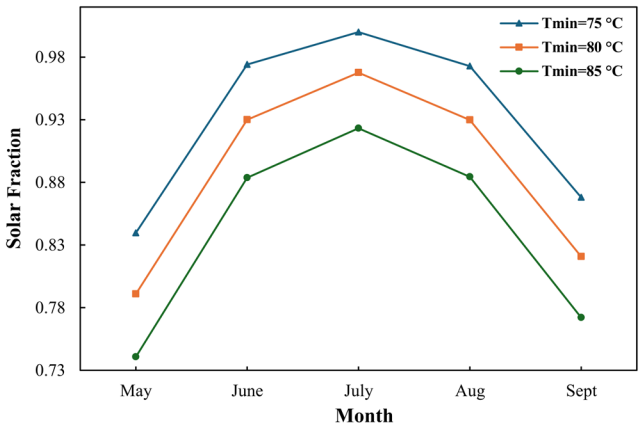

Figure 13. Solar fraction variation with months at different minimum load temperatures for Mosul

3.5 Effect of collector tilt angle

Figure 15 illustrates the variation in solar fraction of the double-glazing flat plate collector across different months (May to September) for varying collector areas in Baghdad and Mosul. The comparison is made between the fixed collector tilt angle (15 degrees below the latitude angle) and the monthly optimum tilt angle recommended by Evans [22]. The results show that, for Baghdad, using the optimum tilt angle results in an average improvement of 2.13% in solar fraction compared to the fixed tilt angle. The month with the most significant improvement is June, which shows a 4.07%

increase in solar fraction with the optimum tilt angle. Similarly, for Mosul, the use of the optimum tilt angle provides a 2.14% average improvement in solar fraction. June again stands out as the month with the most pronounced effect, showing a 4.24% increase in solar fraction with the optimum tilt angle. However, the benefits of adjusting the collector to the optimum tilt angle on a monthly basis are not substantial, suggesting that it is more efficient to maintain the collector at a fixed tilt angle of 15 degrees below the latitude angle throughout the study period.

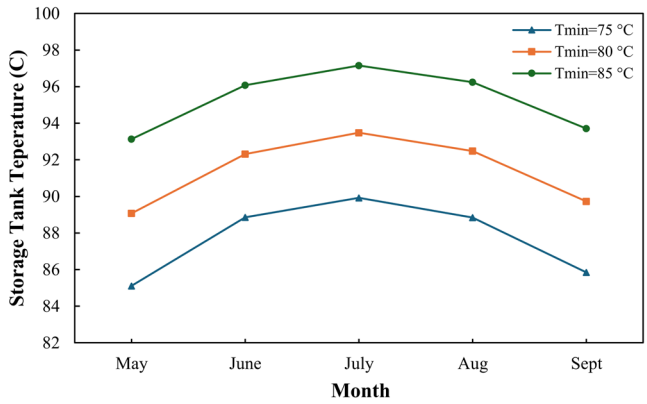

Figure 14. Storage tank temperature variation with months at different minimum load temperatures for Mosul

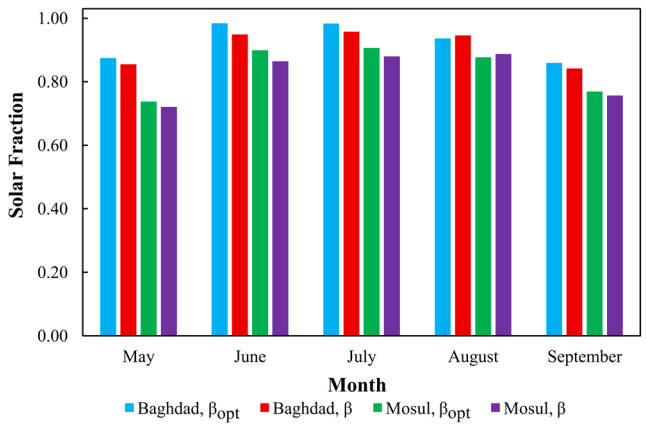

Figure 15. Solar fraction variation with months for the collector optimum tilt angle and the stationary position

3.6 Performance comparison

Figures 16 through 18 illustrate the monthly variation in solar fraction of the double-glazing flat plate collector for four different collector areas, covering the period from May to September in both Baghdad and Mosul. The results show that increasing the collector area consistently leads to higher solar fractions throughout the months. The mean solar fraction tends to peak in July, with lower values observed in May and September. Moreover, increasing the collector area from 40 m² to 55 m² will cause a notable average relative improvement in solar fraction 23.76% for Baghdad and 24.43% for Mosul, for the studied months. Figure 19 shows a comparison between the average solar fraction for the whole studied period with various collector areas. The average solar fraction for both Baghdad and Mosul shows an increasing trend as the collector area increased from 40 m² to 55 m². It is also noted that the average solar fraction for Baghdad was about 2.66% higher than that of Mosul. In addition, the solar fraction will reach 100% for collector areas higher than 55 m² for both cities.

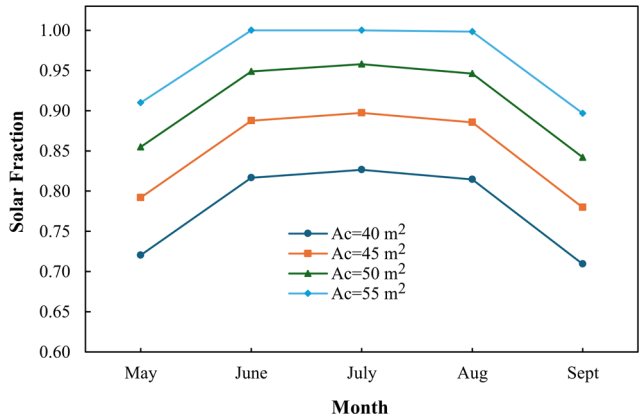

Figure 16. Solar fraction variation with months and collector area for Baghdad

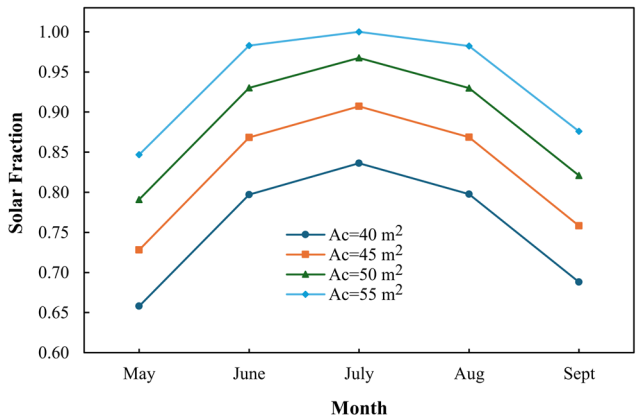

Figure 17. Solar fraction variation with months and collector area for Mosul

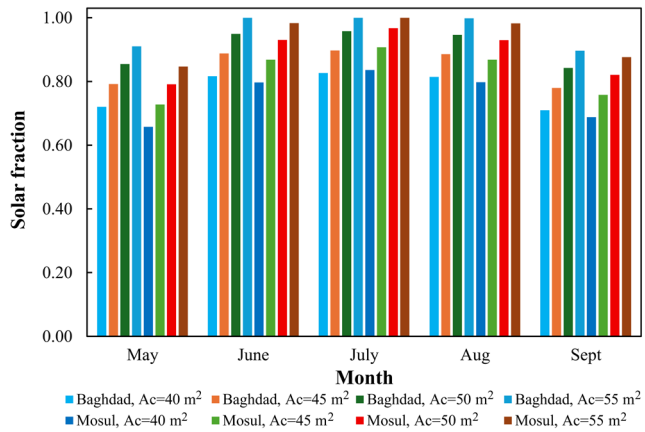

Figure 18. Solar fraction variation with months at different collector areas

3.7 Economic analysis

Solar energy systems are generally characterized by their high initial investment and low operating expenses. To estimate the payback period, it is necessary to calculate the total annual energy savings achieved by the system. The payback period (PB) can be evaluated using Eq. (34) [23]:

$$PB = \frac{log\left[\frac{C}{E_{100}}\frac{i}{+1}\right]}{log\left[1+\frac{i}{100}\right]} \quad (34)$$

Furthermore, some other basic assumptions must be made in the economic analysis, such as maintenance and installation costs and energy inflation. The maintenance cost is taken as 1% of the total investment cost, and the installation cost is 12% of the equipment cost. The equipment costs are presented in Table 3. The annual rate of energy inflation is assumed to be around 2% [24]. The total annual energy savings during the operation period from May to September is about 4820 MWh and electricity cost is 0.33 $/kWh, with these parameters and using Eq. (34) to calculate the payback time, the estimated payback time is around 8 years, which is an acceptable value for solar cooling systems.

Table 3. The costs of equipment

Equipment	Cost
Absorption chiller	500 $/kW
Flat plate solar collector	120 $/m²
Storage tank	790 $/m³
Cooling tower	65 $/kW
Auxiliary heater	50 $/kW

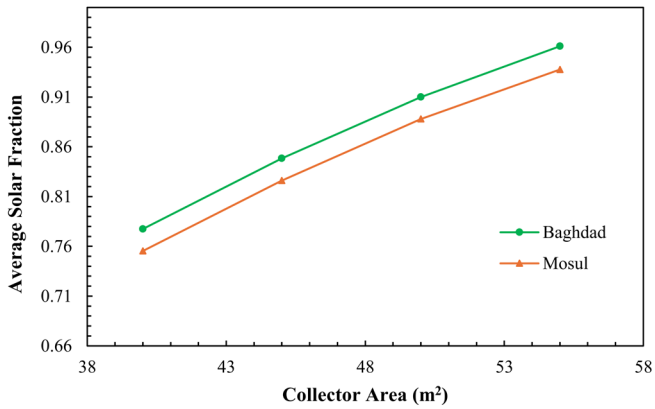

Figure 19. Variation of average solar fraction with collector area

4. CONCLUSIONS

This study evaluated the performance of solar-driven absorption cooling systems for two major Iraqi climates (Baghdad and Mosul) using the $\bar{\phi} - f$ chart method as a simplified modeling technique. Based on the simulation results, the following conclusions can be drawn:

1. Collector glazing type significantly affects performance. Double-glazed flat-plate collectors consistently achieved higher solar fractions than single-glazed ones, with average improvements of about 36%–38%. A collector area above 55 m² allows the system to reach nearly 100% solar fraction during the summer months.
2. System thermal losses were found to have a noticeable impact on efficiency. Increasing the collector area substantially reduced tank and heat exchanger losses by up to 68% in Baghdad and 60% in Mosul, leading to solar fraction increases exceeding 23%.
3. Minimum load temperature variations showed a trade-off between energy availability and system requirements. Raising the generator's minimum operating temperature by 5 °C caused an average 9–11% decline in solar fraction, while slightly increasing storage tank temperature.
4. Changes in the tilt angle of the collectors had a marginal effect on the efficiency. The increase in the solar fraction was about 2% on average, which is an insignificant amount. A constant tilt angle of 15° lower than the latitude is therefore justifiable for such systems.
5. A comparison of the performance of the systems between the two cities showed that the system in Baghdad performed slightly better than that in Mosul, with an average difference of about 2.6% in the solar fraction due to higher solar radiation.
6. Economic analysis revealed that, despite high initial costs, the system has a payback period of about 8 years, which is a reasonable period. Therefore, the system can be considered to be economically feasible for residential applications in Iraq.

In summary, the study demonstrates that the $\bar{\phi} - f$ chart method can serve as a practical design tool for Iraq's climatic conditions, minimizing computational cost while accurately predicting seasonal solar fraction trends. Furthermore, solar thermal absorption systems, when well-designed, can satisfactorily serve the cooling requirements in Iraq weather. Double glazed collectors of adequate surface area present the best performance and economics and could facilitate the move to environmentally friendly, low carbon, solar cooling technology in Iraq.

REFERENCES

[1] Pani, A., Shirkole, S.S., Mujumdar, A.S. (2022). Importance of renewable energy in the fight against global climate change. Drying Technology, 40(13): 2581-2582. https://doi.org/10.1080/07373937.2022.2119324

[2] Kalogirou, S.A. (2024). Solar Energy Engineering: Processes and Systems. Academic Press. https://doi.org/10.1016/C2021-0-02041-1

[3] Klein, S.A. (1978). Calculation of flat-plate collector utilizability. Solar Energy, 21(5): 393-402. https://doi.org/10.1016/0038-092X(78)90171-8

[4] Klein, S.A., Beckman, W.A., Duffie, J.A. (1976). A design procedure for solar heating systems. Solar Energy, 18(2): 113-127. https://doi.org/10.1016/0038-092X(76)90044-X

[5] Klein, S.A., Beckman, W.A. (1979). A general design method for closed-loop solar energy systems. Solar Energy, 22(3): 269-282. https://doi.org/10.1016/0038-092X(79)90142-7

[6] Klein, S.A., Beckman, W.A., Mitchell, J.W., Duffie, J.A., et al. (2004). TRNSYS 16–A TRaNsient system simulation program, user manual. Solar Energy Laboratory. Madison: University of Wisconsin-Madison.

[7] Orgill, J.F., Hollands, K.G.T. (1976). WATSUN—A solar heating simulation and economic evaluation program. User's manual. Technical Report, University of Waterloo, Ontario (Canada).

[8] Polysun. (2008). User Manual for Polysun 4. Vela Solaris AG, Rapperswil.

[9] Lund, P.D., Peltola, S.S. (1992). SOLCHIPS—A fast predesign and optimization tool for solar heating with seasonal storage. Solar Energy, 48(5): 291-300. https://doi.org/10.1016/0038-092X(92)90057-H
[10] Joudi, K.A., Abdul-Ghafour, Q.J. (2003). Development of design charts for solar cooling systems. Part I: Computer simulation for a solar cooling system and development of solar cooling design charts. Energy Conversion and Management, 44(2): 313-339. https://doi.org/10.1016/S0196-8904(02)00045-6
[11] Joudi, K.A., Abdul-Ghafour, Q.J. (2003). Development of design charts for solar cooling systems. Part II: Application of the cooling *f*-chart. Energy Conversion and Management, 44(2): 341-355. https://doi.org/10.1016/S0196-8904(02)00044-4
[12] Alhadithie, A.M.H., Barwari, R.R.I. (2024). Investigation into the feasibility of using solar-powered household air conditioner in the Kurdistan Region of Iraq. Ecological Engineering & Environmental Technology, 25(7): 80-93. https://doi.org/10.12912/27197050/188009
[13] Dawood, A.S., Yousif, H.A. (2013). Optimization of solar-driven of a small absorption air conditioning system. Al-Rafidain Engineering Journal (AREJ), 21(4): 42-56. https://doi.org/10.33899/rengj.2013.77270
[14] Abusaibaa, G.Y., Al-Aasam, A.B., Al-Waeli, A.H.A., Al-Fatlawi, A.W.A., Sopian, K. (2020). Performance analysis of solar absorption cooling systems in Iraq. International Journal of Renewable Energy Research, 10(1): 223-230. https://www.ijrer.ijrer.org/index.php/ijrer/article/download/10472/pdf.
[15] Duffie, J.A., Beckman, W.A. (2013). Solar Engineering of Thermal Processes. John Wiley & Sons, Inc. https://doi.org/10.1002/9781118671603
[16] Erbs, D.G., Klein, S.A., Duffie, J.A. (1982). Estimation of the diffuse radiation fraction for hourly, daily, and monthly-average global radiation. Solar Energy, 28(4): 293-302. https://doi.org/10.1016/0038-092X(82)90302-4
[17] Reddy, T.A. (1987). The Design and Sizing of Active Solar Thermal Systems. Oxford: Clarendon Press.
[18] Klein, S.A. (2018). Engineering Equation Solver (EES) V10, F-Chart Software, Madison, USA. http://www.fchart.com.
[19] Iraqi Agrometeorological Center, Ministry of Agriculture, Iraq. https://www.agromet.gov.iq/eng/index.php, accessed on 11 July 2025.
[20] Tsalikis, G., Martinopoulos, G. (2015). Solar energy systems potential for nearly net zero energy residential buildings. Solar Energy, 115: 743-756. https://doi.org/10.1016/j.solener.2015.03.037
[21] Bellos, E., Tzivanidis, C., Antonopoulos, K.A. (2015) Comparison of two solar driven absorption chillers for air-conditioning in Greece. In 6th International Conference on "Experiments/Process/System Modelling/Simulation/ Optimization" 6th IC-EpsMsO, Athens.
[22] Evans, D.L. (1981). Simplified method for predicting photovoltaic array output. Solar Energy, 27: 555-560. https://doi.org/10.1016/0038-092X(81)90051-7
[23] Falahatkar, A., Khalaji Assadi, M. (2011). Analysis of solar lithium bromide-water absorption cooling system with heat pipe solar collector. Linköping Electronic Conference Proceedings, 57:29: 3889-3896. https://doi.org/10.3384/ecp110573889
[24] Tsoutsos, T., Anagnostou, J., Pritchard, C., Karagiorgas, M., Agoris, D. (2003). Solar cooling technologies in Greece: An economic viability analysis. Applied Thermal Engineering, 23(11): 1427-1439. https://doi.org/10.1016/S1359-4311(03)00089-9

NOMENCLATURE

A_c	collector area, m^2
C	capital cost of installed solar cooling equipment, $
C_{min}	the minimum thermal capacitance rate between the two working fluids, $W \cdot {}^{\circ}C^{-1}$
C_p	stored fluid specific heat, $J \cdot kg^{-1} \cdot {}^{\circ}C^{-1}$
DC	double covers collector
E	energy saving $/yr
f	solar fraction utilized by solar energy
F_R	heat removal factor of collector
f_{tl}	monthly load fraction supplied by solar energy
$\bar{H}$	monthly mean of daily total solar irradiance on a horizontal plane, $J \cdot m^{-2} \cdot day^{-1}$
$\bar{H}_b$	the average daily direct irradiance per month on a horizontal plane, $J \cdot m^{-2} \cdot day^{-1}$
$\bar{H}_d$	the monthly average of daily diffuse solar radiation on a flat horizontal plane, $J \cdot m^{-2} \cdot day^{-1}$
$\bar{H}_o$	average monthly extraterrestrial solar radiation, $J \cdot m^{-2} \cdot day^{-1}$
$\bar{H}_t$	the average daily total solar radiation per month received by the collector, $J \cdot m^{-2} \cdot day^{-1}$)
hrs	time, hr
I_c	value of critical radiation, W
I_{gc}	represent the extraterrestrial irradiance over a specified day, $W \cdot m^{-2}$
I_{min}	minimum value of critical radiation, W
I_{sc}	solar constant, $W \cdot m^{-2}$
i	energy inflation
$\bar{K}_t$	sky clearance index
M	stored fluid mass, kg
N	month total days
n	day number
PB	payback period, yr
Q_{ah}	the heat supplied by auxiliary heater, J
Q_g	monthly generator heat demand, W
Q_L	actual monthly cooling load, J
Q_{solar}	monthly total solar heat supplied by solar energy, J
Q_t	monthly heat demand, J
Q_{st}	energy lost from storage tank, J
$\bar{R}$	the ratio of average daily global radiation per month on a tilted plane to that on horizontal plane
$\bar{R}_b$	the ratio of extraterrestrial radiation on the tilted surface to that on the horizontal surface for a month
$R_{b,n}$	the proportion of beam irradiance on a tilted plane relative to that on a horizontal plane at solar noon
R_n	the noon radiation ratio between a tilted surface and a horizontal surface
$r_{d,n}$	monthly mean radiation to the mean diffuse radiation at noon time, $day \cdot hr^{-1}$
$r_{t,n}$	monthly mean radiation to the mean total radiation at noon time, $day \cdot hr^{-1}$
STC	specific storage capacity, $kg \cdot m^{-2}$
SC	single cover collector

$\bar{T}_{avg}$	the environmental temperature, ℃
$\bar{T}_{env}$	environment storage temperature, ℃
$\bar{T}_i$	useful energy temperature, ℃
$\bar{T}_{min}$	useful energy temperature at minimum value, ℃
$(UA)_{st}$	storage tank's total thermal conductance, W·℃$^{-1}$
U_L	collector loss coefficient, W·m^{-2}·℃$^{-1}$
$\bar{X}_c$	dimensionless critical level of solar collector
$\bar{X}_{c,min}$	dimensionless critical level of solar collector at minimum value

Greek symbols

β	collector tilt angle
δ	declension angle
ε_L	heat exchanger effectiveness.
$\bar{\phi}$	average utilizability of collector
$\bar{\phi}_{max}$	maximum average utilizability collector
λ	latitude angle
ρ	ground reflectance
θ_b	solar beam angle of incidence
ω_s	sunset hour angel
ω_{ss}	month unit time, s
$(\overline{\tau\alpha})$	average transmissivity-absorptivity product
$(\overline{\tau\alpha})_n$	average transmissivity-absorptivity product at normal incidence